Strategic deployment of urban trees to achieve thermal resilience in a Canadian community

Lili Ji[1] (✉), Abhishek Gaur[1], James Voogt[2], E. Scott Krayenhoff[3]

1. Construction Research Center, Nation Research Council Canada, Ottawa, ON, Canada
2. Department of Geography and Environment, Western University, London, ON, Canada
3. School of Environmental Sciences, University of Guelph, Guelph, ON, Canada

Abstract

Climate change and urban heat islands are intensifying the frequency and severity of heatwaves, emphasizing the need for resilient and sustainable strategies to cool urban outdoor and indoor spaces. Urban trees are identified as an effective solution, yet limited studies address how different tree deployment strategies enhance building thermal resilience against heatwaves. This study examines the impact of strategic urban tree deployment on building thermal resilience across a neighborhood in London, Canada. Two deployment strategies are assessed: a straightforward strategy based on outdoor temperature hotspots, and a more complex strategy based on building indoor heat stress. The analysis incorporates tree growth and its effect on canopy coverage. A coupled microclimate-building performance simulation evaluates outdoor and indoor thermal conditions, with thermal resilience quantified using a novel method integrating microclimate effects, heat stress intensity, and exposure duration. Results indicated that when canopy coverage increases from 6% to the Nature Canada-recommended 30%, both strategies achieve similar maximum reductions in building surrounding outdoor air temperature (4.0 °C) and Standard Effective Temperature (6.9 °C), as well as comparable reductions in indoor thermal stress. However, at lower canopy coverage levels (≤20%), the indoor based strategy achieves a more uniform resilience distribution and enhances thermal resilience for the majority of buildings with poorer baseline conditions. At 30% canopy coverage and above, the differences between the two strategies become less pronounced, making tree deployment based on outdoor temperature hotspots a straightforward yet effective strategy for improving neighborhood thermal resilience.

1 Introduction

Climate change poses a significant global threat, leading to an increase in natural hazards such as heatwaves, wildfires, floods, droughts, and other disasters (Birkmann et al. 2022). Heatwaves are becoming more frequent and severe, exacerbated by global warming and urban heat island effects (UHIs) (Krayenhoff et al. 2018; Shu et al. 2023a, b). The implementation of cooling strategies in urban settings has become essential for fostering livable and sustainable cities (Lu et al. 2023). Evaluating and optimizing the effectiveness of cooling strategies to enhance resilience of buildings and neighbourhoods against heatwaves is important to maintain a safe environment for urban residents (Hong et al. 2023; Ji et al. 2024).

Green infrastructure plays an important role in mitigating the impacts of heatwaves in urban environments. Among various types of green infrastructure, trees are widely employed in urban areas and have direct impact on microclimate and, subsequently, on the indoor thermal condition and occupant's thermal comfort. The influence of trees on the microclimate includes not only cooling effects through evapotranspiration and shading (Hsieh et al. 2018; Amitrano et al. 2019) but also heating effects due to longwave radiation trapping and wind blockage (Shu et al. 2016; Makvandi et al. 2019; Meili et al. 2021). Previous studies

E-mail: Lili.Ji@nrc-cnrc.gc.ca

have explored how adding trees can impact the microclimate under different scenarios, such as the comparison in shallow and deep street canyons (Coutts et al. 2016), and the cooling benefits under different weather conditions (Locke et al. 2024) and scales (Ziter et al. 2019). The tree canopy coverage (TCC), an indicator of urban trees for linking their effects with multi-scale thermal performance, has been widely adopted. Studies have quantified the TCC increase on urban cooling (Krayenhoff et al. 2021), outdoor thermal comfort (Li et al. 2023), and reducing summer death (Iungman et al. 2023). Studies have suggested that at least 30% TCC in urban area provides cooling benefits (Konijnendijk 2023), improves residents' sleep quality, and prevents cardiometabolic diseases (Astell-Burt and Feng 2020a, 2020b). Based on these findings, Nature Canada (Nature Canada 2022) has recommended achieving 30% TCC in all neighbourhoods across the country.

It is known that the tree size and locations have significant impact on their efficiency in cooling the outdoor and indoor environment in urban areas (Tsoka et al. 2021). With the same coverage area, strategic tree deployment is recommended to more effectively improve local thermal comfort (Morakinyo and Lam 2016; Hsieh et al. 2018). Different considerations are adopted in tree deployment strategies depending on whether the focus is on improving the outdoor or indoor environment. When aiming to improve the outdoor urban microclimate, studies indicated that placing trees at the right locations is important (Shaamala et al. 2024). Research has found that instead of spreading them evenly, the cooling effect can be maximized when trees are placed at hotspots (Shaamala et al. 2024) or on the leeward side of an area, relative to the prevailing wind direction (Hao et al. 2023). On the other hand, when aiming to improve the building indoor thermal condition, studies have suggested that placing the trees close to the buildings can effectively mitigate overheating in building spaces near the trees. For example, trees located at the building courtyard could decrease the number of discomfort hours in the building thermal zones around the courtyard space (Darvish et al. 2021). Studies also shown that the cooling effects of trees on buildings are mainly contributed to the radiative shading on the exposed building façades, which reduces solar radiation absorption and heat transfer (Tsoka et al. 2021), and therefore optimizing the extent of tree shading on the walls of buildings could maximize the reduction in building cooling load (Mcpherson et al. 1988; Jaffal et al. 2012; Hsieh et al. 2018).

Thus, research commonly suggests two tree deployment strategies: placing trees in outdoor hotspots or near buildings with high indoor heat stress. Deploying trees based on outdoor hotspots in a neighbourhood is a straightforward strategy, and through the interactions between outdoor microclimate and indoor environment, it is expected to also mitigate indoor heat stress. However, the efficiency of this strategy in improving indoor conditions has not been quantified, and there are no comparative studies on the effectiveness of the two strategies (outdoor-based and indoor-based) in enhancing building thermal resilience against summer heatwaves. These quantification and comparison can help determine whether deploying trees at outdoor hotspots in a neighbourhood is an efficient strategy for enhancing building thermal resilience, and whether building simulations, to obtain indoor conditions, are necessary when planning tree deployment in a neighborhood. Addressing these questions could support more effective investments of labor, time, and financial resources in tree deployment within neighborhoods. In addition, exploring methods for quantifying building thermal resilience is also needed. The concept of "resilience" defines the capacity of a subject to anticipate, absorb, adapt to, and/or rapidly recover from a disruptive event (Cabinet Office 2011). Building thermal resilience against heat events can be defined as a building's capacity to withstand disturbances from heatwaves and its adaptability to achieve a robust and rapidly recovering building system (Ji et al. 2023). As such, the quantification of building thermal resilience involves a multi-phase consideration including during and post-heatwave, while accounts for the magnitude of indoor heat stress, as well as the exposure and recovery time. Previous studies provide qualitative or quantitative definitions for individual building thermal resilience (Attia et al. 2021; Zhang et al. 2021), and have calculated building thermal resilience by integrating heat stress indices over the exposure and recovery time at different hazard levels (Homaei and Hamdy 2021; Rahif et al. 2022; Ji et al. 2023). These studies have advanced the resilience concept in building thermal evaluations. However, at a neighbourhood scale, outdoor microclimate has significant impact on building indoor environment, which needs to be accounted for when evaluating thermal resilience (Hong et al. 2023). While some studies have aggregated individually simulated building resilience profiles to calculate thermal resilience at an urban scale (Krelling et al. 2023), the impact of the microclimate is overlooked. Thus, resilience evaluations should consider both microclimate effects on building thermal conditions and comprehensive resilience metrics that account for the intensity and duration of heat stress exposure and recovery.

The microclimate effects of trees at the neighbourhood scale can be modeled with various approaches, such as energy balance models (EBM) and detailed computational fluid dynamics (CFD) models (Ji et al. 2024). Some CFD-based models, such as ENVI-met (2024), incorporate built-in vegetation models, making them widely used for simulating microclimate impacts of greenery. Other

CFD-based tools, including Fluent (Guo et al. 2022) and OpenFOAM (Hadavi and Pasdarshahri 2021), and EBM-based models including multi-layer urban canopy model (UCM) (Erell and Zhou 2022) and single-layer UCM (Zheng et al. 2023), have also been used, though they require customized vegetation models. Microclimate impact on building conditions can be assessed by integrating microclimate simulations with building performance modeling, through a one-way data exchange co-simulation approach (Ji et al. 2024). EnergyPlus is the predominant tool for building performance simulations, particularly for co-simulations with microclimate models (Ji et al. 2024). Therefore, this study adopts the microclimate and building simulation approach to evaluate the effects of tree deployment strategies on building thermal resilience.

Overall, the objectives of this study are to

- evaluate the relative effectiveness of two different urban tree deployment strategies based on both building outdoor and indoor thermal conditions,
- identify best practices to improve the thermal resilience of buildings across a neighborhood, and
- quantify building thermal resilience by integrating microclimate effects, heat stress intensity, and exposure duration.

The remainder of the paper is organized as follows. Section 2 introduces the methodology. Starting from an overview of the workflow, Section 2 details the study area, the microclimate and building simulation models, including the integration of microclimate data into building performance simulations, and measurement datasets used for evaluating and forcing the models, as well as the quantification method of thermal condition and resilience. Section 3 presents the results of model evaluation, assesses the consistency of prioritized locations for tree deployment based on outdoor and indoor conditions, and compares the changes in building thermal conditions and thermal resilience under different tree canopy coverage levels and tree

deployment strategies. Section 4 presents the discussions and conclusions.

2 Methodology

An overview of the methodology is presented in Figure 1. To evaluate the effects of tree deployment strategies on building thermal resilience in a Canadian neighbourhood, microclimate models are developed and the models are evaluated by comparing with the traverse measurement data. Buildings in the neighbourhood are represented with an archetype building model, with microclimate modeling results serving as boundary conditions for the building simulations. Considering the effects of tree growth, buildings located at outdoor hotspots and those experiencing high indoor heat stress are identified. The buildings are ranked based on the level of the outdoor and indoor heat conditions, respectively. The rankings of these buildings are evaluated to determine whether significant differences exist between them. Based on these findings, trees are added and deployed in the identified locations by two strategies. Changes in outdoor and indoor thermal conditions are analyzed using air temperature and Standard Effective Temperature (SET). The building thermal resilience is further quantified with a novel method that integrates microclimate effects, heat stress intensity and exposure time at different hazard levels. The building thermal resilience across the neighbourhood is analyzed.

2.1 Study area

In this study, two adjacent sites located in the Uplands neighbourhood in the northeast section of London, ON, Canada (43°2′8″ N, 81°15′54″ W) are used to evaluate the urban microclimate model. These sites were selected because truck-based traverse measurements were conducted at the two sites on Sep. 23–Sep. 24, 2017, and the microscale
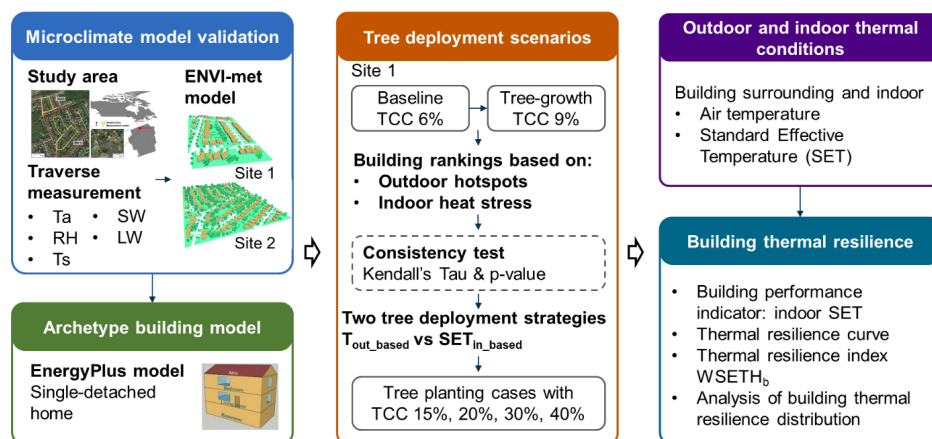

Fig. 1 Overview of the methodology

models used in this work are evaluated with measurement data collected in the area. The traverse routes are highlighted in yellow in Figure 2.

According to the Köppen climate classification system, the city of London is located in the Dfb (Humid Continental Mild Summer) climate zone (Kottek et al. 2006). In late September, 2017, London experienced a heatwave when outdoor air temperatures in the city peaked at 32.2 °C, the highest for the city on that date since 1959 (Environment Canada 2024). The Uplands neighbourhood is predominantly composed of single-detached houses, which constitute 77% of its residential structures. The vegetative landscape is primarily characterized by deciduous trees. The trees located in the front yards and along the street are of a younger age and smaller stature, while the backyards are host to larger, mature trees. As shown in Figure 2, during the time of the measurement campaign, Site 1 had sparse tree coverage, whereas Site 2 had denser foliage with larger mature trees. In some areas of Site 2, the tree crowns cover the entire width of the street, providing extensive shade and contributing to thermal comfort of the community.

While urban microclimate model evaluation is performed over both Site 1 and Site 2, the detailed evaluation of effectiveness of increasing tree canopy coverage (TCC) is conducted over Site 1, as it has a lower tree cover level. Since the two sites are close to each other, the response to increasing TCC on thermal resilience of neighborhoods will likely be similar.

2.2 Microclimate model

2.2.1 ENVI-met model

In this study, the modeling of urban microclimate over the two sites is conducted using ENVI-met V5.6.1 (ENVI-met 2024), a widely used and actively researched three-dimensional climate simulation tool that can model the interactions between atmosphere, soil, vegetation and buildings at a micro level. In the atmosphere model (Simon 2016), the wind field's spatial and temporal changes are computed using the non-hydrostatic three-dimensional Navier-Stokes equation. The distribution of ambient air temperature and specific humidity is calculated in connection with the vegetation model. This includes internal sources and sinks to account for localized variations. The model captures exchange processes between vegetation and the atmosphere, ensuring a realistic representation of their interactions. Turbulence is modelled by accounting for both the generation and dissipation of turbulent energy. Vegetation affects the radiation through the changes in sky view factor (Darvish et al. 2021), direct/diffuse shortwave radiation, and downward/upward longwave radiation. The underside of the atmosphere model is connected to the soil model (Simon 2016), where hydrological and thermal processes up to a depth of 5 meters are computed (Ji et al. 2024). ENVI-met adopts Darcy's law to calculate the soil hydraulic state, accounting for processes such as evaporation, water exchange within the soil mass, and water uptake by plant roots (Wang et al. 2021). Vegetation geometries are modeled using Lindenmayer-System ("LSystem"), a method that reflects self-similarity in natural vegetation patterns (Lindenmayer 1968), with which leaf area densities and shapes are resembled with high accuracy (Sinsel 2021). The radiation model has been enhanced in recent versions with a ray-tracing approach, allowing for the accurate accounting of received radiation from reflections of surrounding objects (Sinsel 2021). ENVI-met modeling, along with its co-simulation with mesoscale or building-scale models, has been successfully validated in the literature (Ji et al. 2024). Figure 3 presents the ENVI-met models of
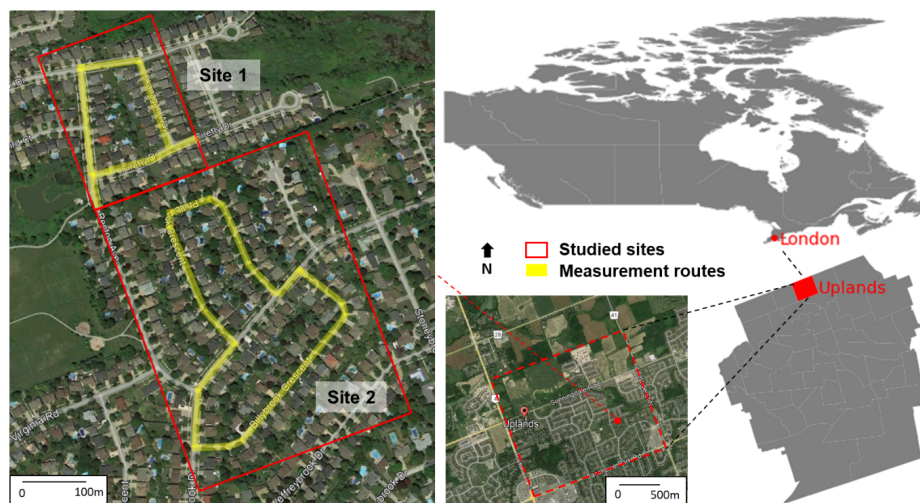

Fig. 2 Locations of the two studied sites and traverse measurement routes
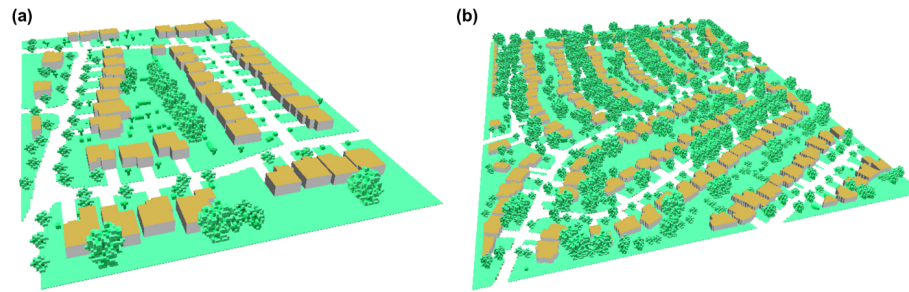
Fig. 3 ENVI-met models of (a) Site 1 and (b) Site 2

the two sites, both of which are used for model evaluation, while the increase of TCC is conducted for Site 1.

Table 1 lists the geometry settings used in the models. Building height specifications and tree species data are based on Krayenhoff et al. (2020). The detailed geometry of street and backyard trees are determined through measurements and visual estimations from Google Earth Pro's historical map of 2017, complemented by data from the ENVI-met Albero module. For Site 1, the horizontal domain is 180 m × 250 m, with the individual grid sizes of 1 m × 1 m × 1 m. For Site 2, the horizontal domain covers an area of 350 m × 440 m, also with the individual grid sizes of 1 m × 1 m × 1 m. According to ENVI-met modeling guidelines, the distance between the model border and the nearest building should be at least half the height of the building, to prevent the building cells from blocking or channeling wind flow. Therefore, each model area boundary is set with a minimum of six grids of open space to ensure adequate airflow. The vertical dimension of the model is divided into 40 grids, with the lowest grid box further segmented into five sub cells. Above a height of 12 m, the grid size increases at a telescoping rate of 20%.

Table 2 lists the thermal property settings for surfaces and vegetation in the simulation models, which incorporate the information from (Krayenhoff et al. 2020), and the database for soil/ground, wall/roof and vegetation provided by ENVI-met.

2.2.2 Measurement data for model evaluation

Mobile measurements within the Uplands neighbourhood were carried out on Sept. 23–Sept.24, 2017. The traverse routes are highlighted in yellow in Figure 2. The measurement campaign utilized a truck equipped with an upward-facing fast response pyranometer and pyrgeometer, and infrared radiometer for the measurement of road surface temperature (Krayenhoff et al. 2020; Stastny et al. 2023). The equipment was affixed to a temporary rack, which was installed in the bed of a conventional pickup truck. For certain traverses, additional imaging instruments, including a Digital Action Camera and a thermal imager, were deployed to acquire detailed insights into the road surface materials and the variability of surface temperatures. Air temperature and relative humidity at 2.65 m height were measured. Truck routes were driven at separate times within the measurement period. Detailed description of the sensors, precision and parameters of the measurement can be found in Appendix A.1. The Appendix is in the Electronic Supplementary Material (ESM) in the online version of this article

2.2.3 Tree-growth and tree-planting cases

To explore how the tree growth and tree planting can lead to an increased TCC and affect the microclimate in the neighbourhood and subsequently influence indoor thermal conditions, cases with different tree sizes and increased

Table 1 Geometry settings in the ENVI-met models

Geometry	Height (H) (m)		Crown width (W) (m)		Leaf area density (LAD) (m^2/m^3) at height (m)	
	Site 1	Site 2	Site 1	Site 2	Site 1	Site 2
Building	6.0	5.0	/	/	/	/
Street tree	6.4	10.4	5.3	6.7	0.15–1 (at 5.5m)	0.2–1.5 (at 5.5m)
	5.0	5.8	3.0	4.9	0.3–2 (at 4.5m)	0.1–2 (at 4.5m)
Backyard tree	15.8	20.1	12.8	14.5	0.2–1.5 (at 5.5m)	0.2–2.7 (at 5.5m)
	10.4	15.8	6.7	12.8	0.2–1.5 (at 5.5m)	0.2–1.5 (at 5.5m)
Hedge	2.0	4.0	/	/	0.55 (at 1m)	0.55 (at 1m)
Grass	0.1	0.1	/	/	0.3 (at 0.1m)	0.3 (at 0.1m)

Table 2 Thermal property settings in the ENVI-met models

Parameter	Street/driveway	Wall	Roof	Vegetation
Albedo	0.15	0.25	0.13	0.18 (tree) 0.2 (grass/hedge)
Emissivity	0.91	0.9	0.91	0.96 (tree) 0.97 (grass/hedge)
Heat capacity (MJ/(m³·K))	1.94	2.05	1.44	/
Thermal conductivity (W/(m·K))	0.75	1.25	1.0	/
Deep (internal) temperature (K)	292	/	/	/

number of trees with their strategic deployment are modeled. In the tree-growth case, the locations of the trees remain the same as the baseline case, while increments are made to the height, crown size, and LAD of current trees in the neighborhood. The increments are based on data from the ENVI-met Albero module and visual estimations from Google Earth Pro's 2023 maps (compared to the maps of 2017), referencing various growth stages of the Norway maple tree type—a predominant tree species in the studied neighbourhood. In the tree-planting cases, the number of trees is increased while maintaining proportion of the four tree types as observed in the tree-growth case. The four tree types and their specifications are listed in Table 3. To strategically deploy the trees and maximize their positive impact on indoor thermal conditions, the deployment of new trees is informed by analyses of either outdoor temperatures or indoor thermal conditions observed in the tree-growth case (see Section 3.2). Their effectiveness in improving building thermal condition and resilience is thereafter compared (see Section 3.3). The TCC in each designed case is calculated, with a maximum TCC set at 40%. Previous studies generally report that the optimal air temperature reduction in residential areas is achieved when tree canopy coverage (TCC) is below 40% (Yang et al. 2018; Wu et al. 2019; Ouyang et al. 2020). The TCC, number of trees and their increments are summarised in Table 4. The TCC for each case is calculated by summing the horizontal canopy coverage area of individual trees, while ensuring that in cases of canopy overlap, only a single layer of coverage is

Table 3 Four tree types and their specifications in the neighbourhood

Tree type	Tree location	Crown width (m)	Height (m)	LAD at height (m)
a	Backyard	14.51	20.13	0.2–2.7 at 5.5m
b	Backyard	12.83	15.82	0.2–1.5 at 5.5m
c	Street side	5.95	10.36	0.15–1 at 5.5m
d	Street side	4.91	6.39	0.2–1.5 at 5.5m

Table 4 Tree configurations in tree-growth and tree-planting cases

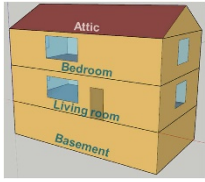| Case	TCC	Tree type	Number of trees	Increment in number of trees
Tree-growth case	9%	a	8	0
		b	9	0
		c	39	0
		d	30	0
Tree-planting case A	15%	a	13	5
		b	15	6
		c	64	25
		d	50	20
Tree-planting case B	20%	a	18	10
		b	20	11
		c	87	48
		d	67	37
Tree-planting case C	30%	a	27	19
		b	30	21
		c	129	90
		d	99	69
Tree-planting case D	40%	a	35	27
		b	40	31
		c	172	133
		d	132	102

counted. Consistent boundary conditions and other model settings are used across all scenarios to control variations in modelled microclimate from factors other than trees.

2.3 Building model and building thermal resilience

2.3.1 EnergyPlus model and coupled simulation

A building model of the archetype single-detached home, shown in Table 5 is prepared in EnergyPlus, which is a widely used building performance simulation software (DOE 2024). The building model comprises of four thermal zones: the underground basement, living room on the first floor, bedroom on the second floor, and an attic on the top of the building. In Table 5, the building geometry, envelope configuration, internal heat gains, occupant schedule, infiltration rate, and ventilation control are listed, following the current construction practice for homes based on the National Building Code of Canada (NRC 2015) and National Energy Code of Canada for Buildings (NECB) (NRC 2017). The building model is set as naturally ventilated under a free-running condition following the requirements of the overheating guidelines (Laouadi et al. 2022). The model can therefore represent the general conditions of residential buildings in Canada. More detailed description of the building model can be found in Shu et al. (2022). The usage of the building model can assess the

Table 5 Archetype single-detached home building model used for indoor thermal condition simulation

Component	Material and properties
Geometry	
Footprint area	80.20 m^2
Window	Double clear with Low-E (U = 1.58; VT = 73%; SHGC = 0.67, WWR = 15%)
Roof	Asphalt shingles with attic insulation (RSI 8.2)
Walls	Wood stud with Vinyl cladding (RSI 4.5)
Blinds	Internal blinds (set slat angle as 90° to capture the solar radiation effect)
Internal heat gains	Lighting: 5 W/m^2, equipment 5 W/m^2, hot water: 500 W/person
Infiltration rate	2.32 air changes per hour at 50 Pa
Natural ventilation	Window opening when the outdoor air temperature is lower than the indoor air temperature, and the indoor air temperature is higher than 26 °C; designed ventilation rate: 0.75 L/(s·m^2)
Occupant schedule	Living room: 7:00 to 21:00 Bedroom: 22:00 to 6:00

indoor thermal environment, considering not only internal heat gains but also the influence of the microclimate through heat exchange across the opaque building envelope, solar radiation through windows, and air exchange via infiltration and ventilation.

The EnergyPlus input files (.epw files) at each building location are modified by ENVI-met simulation results so that the effects of microclimate surrounding the buildings are considered in the indoor climate simulation. Since ENVI-met modelling was performed at a 1 m spatial resolution around the building, appropriate data are needed to modify the EnergyPlus input file. Therefore, in the current study, referring to a method by Zhu et al. (2022), the air temperature, relative humidity, dew point temperature, and radiation components including shortwave direct and diffuse radiation, and longwave radiation at 1.5 m of building adjacent grids are extracted at each building location and wind speed, wind direction at 10 m are extracted at each building center. Since the wind speed reflects the local weather conditions of each building rather than the standardized conditions measured by weather stations, the wind speed profile exponent and boundary layer thickness in the building model are adjusted accordingly. The detailed adjustment can be found in Appendix A.2.

2.3.2 Building thermal condition and resilience evaluation

Standard Effective Temperature (SET), a heat stress index,

is used to assess building thermal conditions. Indoor SET is calculated using the simulated indoor parameters—air temperature, relative humidity, and mean radiant temperature—assuming an indoor airflow rate of 0.1 m/s, occupants engaged in sedentary activities (MET = 1), and wearing typical summer clothing (clo = 0.5). SET differs from air temperature as it accounts for humidity, radiation, and human factors. A detailed explanation of the SET calculation is provided in Appendix A.4. In this study, the indoor thermal condition of the occupied thermal zones is evaluated by calculating SET$_{in}$ as the average of the values from living room and bedroom. SET is also used to evaluate the outdoor thermal conditions, which is calculated with BIO-met module of ENVI-met (2024), assuming a person with a body weight of 69.9 kg, body surface area 1.8258 m^2, summer outdoor clothing level of 0.9clo and walking speed of 1.34 m/s (ASHRAE 2017).

For the quantification of building thermal resilience against the heatwave, a novel method is adopted to calculate thermal resilience indices for building multi-zonal and time-integrated evaluations for short-term heat events (Ji et al. 2023). The quantification of building thermal resilience involves several key steps and the explanation of each step is as follows:

1) Selecting a thermal performance indicator

SET is selected as building thermal performance indicator (Hong et al. 2023). According to three SET thresholds, i.e., SET$_{comf}$ = 24.12 °C, SET$_{alert}$ = 28.12 °C, SET$_{emer}$ = 32.12 °C, three hazard levels can be identified: habitable level, alert level, emergency level (Ji et al. 2023). In this study, indoor SET is derived through the co-simulation of microclimate and building models, enabling the incorporation of microclimate impacts into the calculations.

2) Constructing thermal resilience curves

With an outdoor air temperature of 28 °C as the threshold (Laouadi et al. 2020), a heatwave period is considered to occur from 11:00 to 16:00. During and after this period, the indoor SET in each zone (living room and bedroom) in each building presents a similar trend of trapezoid as shown in Figure 4(a), with the absolute values for each zone vary. Each curve consists of two periods including the heat exceedance period (t_0–t_1) and post-heatwave period (t_1–t_2). Divided by the two periods, three hazard levels (Habitable, Alert and Emergency), and exposure time at each hazard level, 12 segments (S1 to S12) are obtained under each resilience trapezoid curve.

3) Calculating thermal resilience indices

The zone-level thermal resilience performance $WSETH_z$ is calculated by summing the areas of the 12 segments, with each segment assigned penalty coefficients to reflect the exposure time effect, as shown in Equation (1).

$$WSETH_z = \sum_1^{12} WSETH_i = \sum_1^{12} SETH_i W_{1,i} W_{2,i} W_{3,i} \qquad (1)$$

$$WSETH_b = \sum \frac{WSETH_{z,j} \times A_j}{\sum_1^N A_j} \qquad (2)$$

where i is the segment counter (1–12), $SETH_i$ is the area of each segment. To reflect the recovery difficulty from exposure to heat, penalty weights are assigned to each of the segments ($SETH_i$) based on three factors: the phase of the event (during or post-heatwave), the hazard level, and the exposure time (Homaei and Hamdy 2021). These values assigned to each segment are shown in Figure 4(b). The higher the penalty weights, the more difficult for the building to recover from exposure to heat (Ji et al. 2023). W_1 represents the recovery difficulty considering the event phase. For example, the penalty value during the heatwave is higher ($W_{1,i=1-6} = 0.6$) compared to the post-heatwave period ($W_{1,i=7-12} = 0.4$), reflecting the greater thermal stress during the heatwave phase. W_2 accounts for the hazard level. The emergency level has the highest penalty value ($W_{2,i=5-8} = 0.7$), indicating the greatest recovery difficulty. The alert level has the moderate penalty value ($W_{2,i=3,4,9,10} = 0.2$), and the habitable level has the lowest penalty value ($W_{2,i=1,2,11,12} = 0.1$). W_3 reflects the recovery difficulty related to exposure time within each hazard level. For instance, during the heatwave at the habitable level, the penalty value for short exposure (S1) is $W_{3,1} = 2$ and for long exposure (S2) is $W_{3,2} = 8$, meaning that extended exposure to a hazard level increases the difficulty of recovery. The specific values of the penalty weights were adopted from the studies of Homaei and Hamdy (2021) and Ji et al. (2023). These studies employed the penalty coefficients within a thermal resilience quantification framework to calculate a multi-phase metric and assess zone-level thermal resilience performance during summertime heatwaves.

Based on the floor area of each room, the weighted average of the zone-level resilience for each building can be calculated using Equation 2, representing the building's thermal resilience performance $WSETH_b$.

where j is the counter of zones in a building, A_j is the floor area of each zone, N is the total number of zones in the building.

3 Results

3.1 ENVI-met model evaluation

The simulation is carried out over a 24-hour period starting from 0:00 on Sep. 23, including a spin-up time of 4 hours. This simulation period is consistent with the common period of CFD simulations (Ji et al. 2024). The boundary conditions during the simulation period are sourced from the Canadian Weather Energy and Engineering Datasets (CWEEDS) (Natural Resources Canada 2022), which provides hourly meteorological data for at least 10 years between 1998 and 2020 for 644 locations across Canada, including London, Ontario. Figure A.3 in the Appendix illustrates the boundary conditions during the simulation period. A pre-processing routine was implemented on the data to align with the specific requirements for boundary conditions set by ENVI-met, as listed in Table A.2. The ENVI-met model is evaluated by comparing model outputs in the baseline case with the measurements reported by (Krayenhoff et al. 2020). Along the traverse measurement routes, air temperature (Ta), relative humidity (RH), downwelling shortwave radiation (SW), and downwelling longwave radiation (LW) at 2.5 m height (sensor height), and the road surface temperature (Ts) were extracted and averaged at the corresponding time points for comparison with the measured data. Figure 5 presents the comparative analyses between the measured and modeled data for Site 1 and Site 2. As shown in Figure 5(a), the measured and modeled mean Ta, RH and Ts closely match in Site 1,
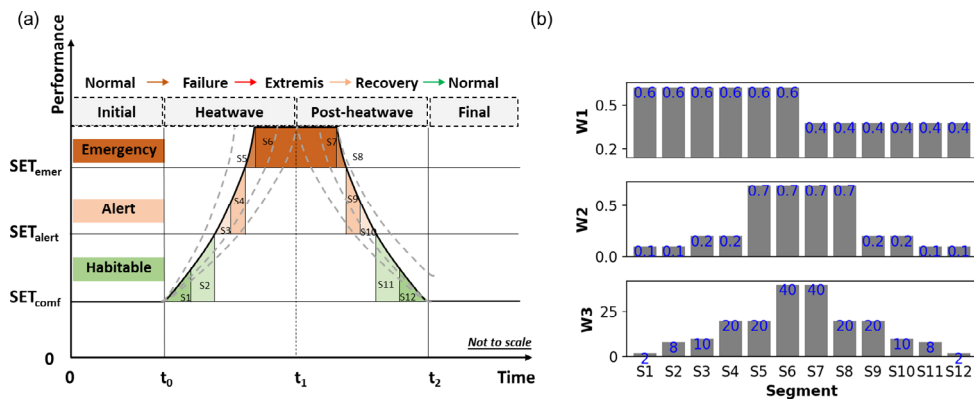

Fig. 4 Important information for evaluating building thermal resilience: (a) the conceptual thermal resilience trapezoid curve and (b) the penalty coefficient values for each segment
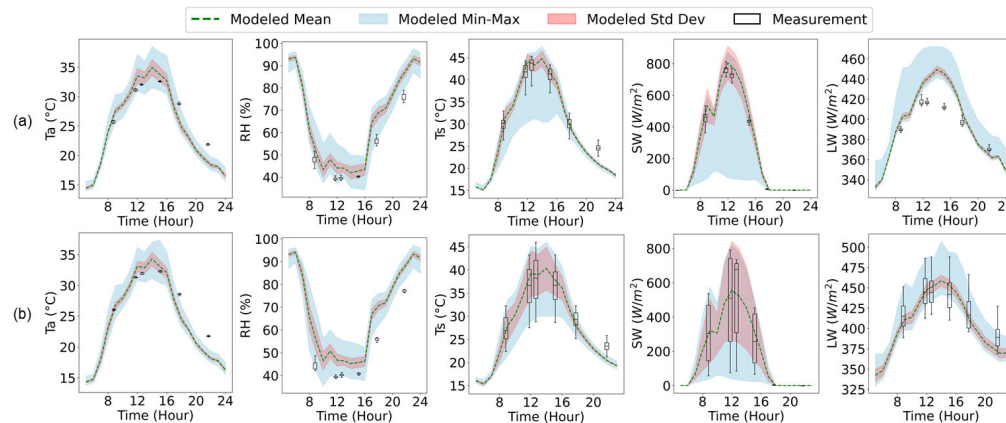
Fig. 5 Comparisons of measured and modeled air temperature (Ta), relative humidity (RH), road surface temperature (Ts), downwelling shortwave radiation (SW), and downwelling longwave radiation (LW) for (a) Site 1 and (b) Site 2

evidenced by the root mean square error (RMSE) values of 1.23 °C, 7.69%, and 1.58 °C, respectively. As shown in Figure 5(b), similar results are obtained from Site 2, with RMSE values for Ta, RH, and Ts of 1.82 °C, 10.60%, and 1.50 °C, respectively. These error levels align with previous validation studies of ENVI-met simulation, which reported RMSE values for Ta, RH and Ts ranging from 1.02 °C to 1.89 °C, 5.68% to 10.60%, and 1.60 °C to 1.98 °C, respectively (Yang et al. 2013, 2021; Huang et al. 2015; Tsoka et al. 2021; Yang et al. 2021; Elraouf et al. 2022; Ge et al. 2023).

Due to the shading effects of trees on the roads, there are variations in the measured Ts, SW, and LW, especially in Site 2, where tree crowns provide extensive shade to the road surface. Figure 5 displays the maximum and minimum modeled values over the road and the standard deviation (Std Dev) of each parameter. The variation of parameters over the road demonstrated the model's ability to capture the effects of tree/building shading as well as building and tree surface radiation. Figure 5(a) shows a discrepancy where modeled downwelling LW radiation slightly exceeds observed values in Site 1 (RMSE = 17.82 W/m²). This discrepancy is attributed the pyrgeometer's positioning 2.75 m above the road surface during measurement, capturing a greater sky view and lesser building view compared to street-level perspectives in the model (Krayenhoff et al. 2020). Therefore, the discrepancy is reasonable. Figure 5(b) shows a better downwelling LW radiation results in Site 2, with an RMSE between modeled and measured values of 10.03 W/m². The denser tree canopy at Site 2 provided shading for both buildings and the sky, making the view from the measurement devices more consistent with the modeled street-level perspective.

Additionally, due to the lower tree density, Site 1 experiences higher thermal stress compared to Site 2, as evidenced by higher surface temperatures and greater solar radiation received. The following sections focus on Site 1,

aiming to evaluate the improvement of neighbourhood thermal resilience through tree growth (Section 3.2) and strategically deploying additional trees (Section 3.3).

3.2 Analysis of tree-growth case

As listed in Table 4, the tree-growth case leads to a TCC of 9% compared to the baseline case of 6%, as well as increments in width and height of trees at the same locations, and changes in LAD at the same heights. To assess its impact on building surrounding conditions, the air temperatures at 1.5 m height from adjacent building grids were extracted, and point-to-point subtraction was performed against the baseline case to determine average and maximum reductions. Since indoor temperatures are uniform within each thermal zone, the subtraction was applied to the mean indoor temperatures of the bedroom and living room zones in corresponding buildings. Compared to the baseline case, the average reduction in building surrounding air temperature (T_{out_sur}. "sur" here is an abbreviation for "surrounding") and indoor air temperature (T_{in}) are 0.2 °C and 0.3 °C, respectively. The spatial maximum reduction in T_{out_sur} and T_{in} are 1.5 °C and 1.7 °C, respectively.

The outdoor and indoor thermal condition distributions for the tree-growth case are shown in Figure 6. Four indices are plotted for 2 PM T_{out} and outdoor SET (SET_{out}) at 1.5 m height, along with T_{in} and indoor SET (SET_{in}). In Figure 6, each building is assigned an index for the purpose of the subsequent analysis. From Figure 6(a), it is evident that T_{out} is lower in the areas directly impacted by prevailing winds, and under mature trees in backyards. Incoming air at this height is primarily warmed through convergence of sensible heat originating from the ground and surrounding surfaces, which have absorbed solar radiation. In areas with trees, shading reduces the heating of the ground and surrounding
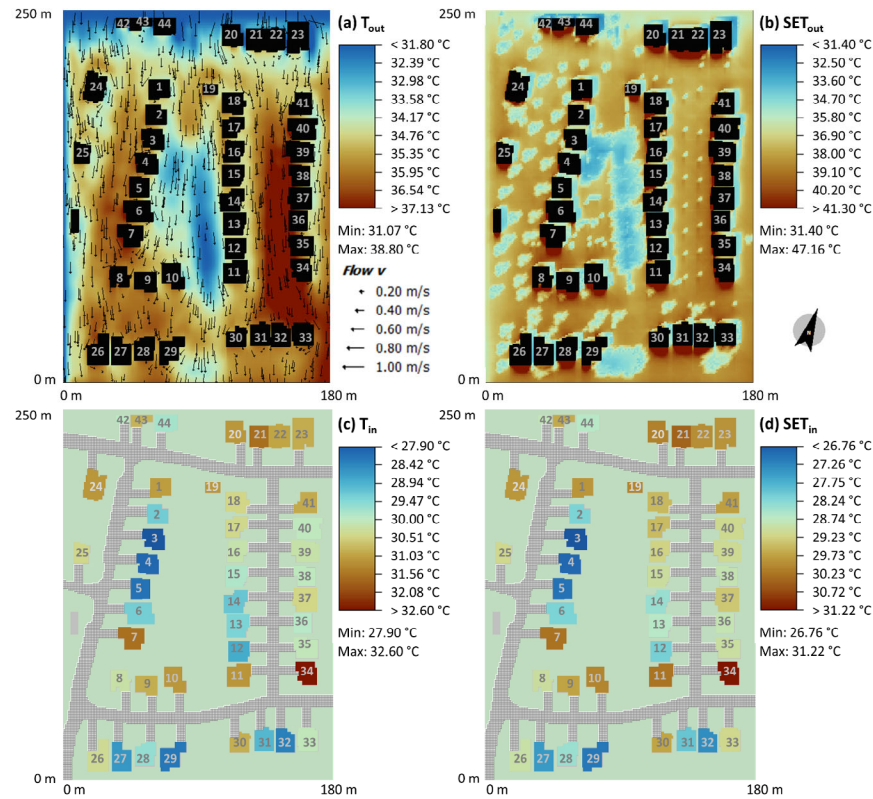
Fig. 6 Mapping at 2 PM of Site 1 of (a) T_{out} and airflow vectors at 1.5 m height, (b) SET_{out} at 1.5 m height, (c) T_{in} of each building, and (d) SET_{in} of each building. The number shown on each building is the building index

surfaces, leading to localized cooling of the air. Trees with larger crown size, height and LAD exhibit more pronounced cooling effects due to their higher evapotranspiration rate and shading effect. Figure 6(b) shows that SET_{out} is lower under the shading of trees and buildings due to the reduced solar radiation, while it is higher on the southern side of buildings. This increase is caused by the warming of adjacent air temperature by the sun-heated facades, direct solar radiation, and reduced air flow, which limits heat dissipation from the human body. The spatial distributions of T_{in} and SET_{in} are similar. In buildings located in areas with fewer trees and high outdoor air temperatures, both T_{in} and SET_{in} are higher compared to the areas where have more and larger trees. This demonstrates the significant impact of tree density and size on both outdoor and indoor thermal conditions.

3.3 Effects of tree deployment strategy

To deploy additional trees at strategic locations, the locations of hotspots in terms of outdoor and indoor conditions need to be identified. To achieve this, the T_{out_sur} and SET_{out_sur} ("sur" here is an abbreviation for "surrounding", referring to the parameters extracted from the building adjacent grids) at 1.5 m height, and the indoor T_{in} and SET_{in} of each

building at all time points are extracted and plotted in Figure 7. The boxes are ordered based on their median values across the one-day simulation period, arranged from lowest to highest. To test whether the order of buildings based on the outdoor and indoor parameters shows significant differences, Kendall's Tau (Shu et al. 2023c) and the associated p-values (Muñoz-Pichardo et al. 2021) were calculated for each pair of rankings and are presented in Table 6. Kendall's Tau measures the degree of agreement between rankings, with a positive value (close to +1) indicating similar rankings and a negative value (close to −1) indicating inverted rankings (Shu et al. 2023c). As shown in Table 6, the Kendall's Tau values are small, ranging from −0.27 to +0.11 suggesting minimal agreement between the ranking orders. Specifically, the value −0.27 indicates a weak tendency toward opposite rankings between the orders based on T_{out_sur} and SET_{in}. This weak opposite ranking

Table 6 Statistic analysis of the building rankings

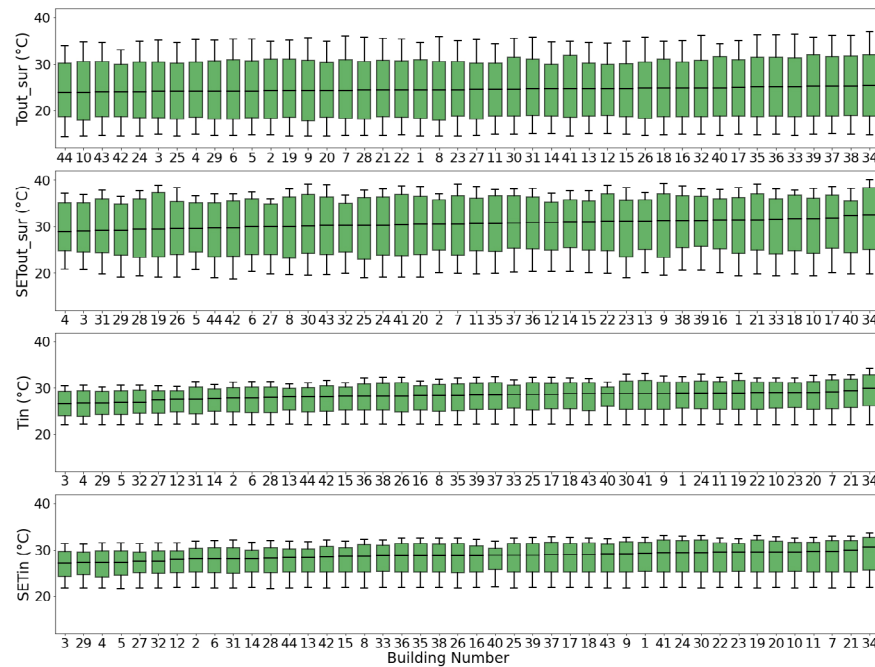| Rankings based on	Kendall's Tau	p-value
T_{out_sur} vs T_{in}	−0.105	0.311
T_{out_sur} vs SET_{in}	**−0.270**	**0.010**
SET_{out_sur} vs T_{in}	0.114	0.275
SET_{out_sur} vs SET_{in}	0.101	0.332

Fig. 7 Variation of T_{out_sur} and SET_{out_sur} surrounding each building, and T_{in} and SET_{in} within each building. Boxes are ordered with median values from low to high (the building index can be referred to Fig. 6)

suggests that microclimatic conditions play a crucial role in shaping indoor and outdoor thermal environments. Areas with lower T_{out_sur} are often more vegetated, which reduces outdoor temperature through shading and evapotranspiration. However, increased vegetation can also limit airflow and radiative heat loss, potentially leading to heat accumulation indoors. Conversely, areas with higher T_{out_sur} tend to have more solar exposure, but stronger convective cooling and better ventilation may help dissipate indoor heat more effectively. Additionally, as noted in Section 2.3, window ventilation is activated when $T_{in} > T_{out}$ and $T_{in} > 26$ °C, allowing passive cooling in buildings located in warmer outdoor areas. To further assess whether the differences in rankings are statistically significant, the p-values associated with Kendall's Tau are analyzed. A p-value of less than 0.05 indicates that the differences are statistically significant (Muñoz-Pichardo et al. 2021). The results show that the ranking orders based on T_{out_sur} and SET_{in} are significantly different, whereas other pairs of rankings do not exhibit systematic differences. Therefore, inconsistency in building rankings based on T_{out_sur} and SET_{in} are observed, leading to different prioritization of tree deployment locations depending on the parameter used.

Based on the above discussion, additional trees can be deployed at locations identified by a straightforward method based on the distribution of building surrounding outdoor temperatures (which can readily be obtained from observations) named the T_{out_based} strategy, as well as based on a more complex method based on indoor heat risk

(communicated by SET) named SET_{in_based} strategy. Table 4 has listed the type and total number of trees, along with TCC in each case. Since these two strategies prioritize buildings differently, the distribution of trees varies between them. The number of additional trees surrounding each building is shown in Table 7. For instance, in the case with 15% TCC, Table 4 has indicated that five Type **a** trees and six Type **b** trees are allocated to backyards, while 25 Type **c** trees and 20 Type **d** trees are deployed along streets. Trees are therefore assigned to backyards or streets sequentially, following the building priority rankings from each strategy. This involves deploying one tree to the backyard or street side of a building at a time until the tree limit is reached. The trees are only added in the backyards and on the street side in front of buildings. The distance between two trees is set to be longer than the sum of their radii to avoid overlapping of tree canopy coverage following Li et al. (2023). Additionally, trees are planted at least 3 meters away from buildings to avoid tree roots damaging building pipelines (Hsieh et al. 2018). The 3D visualization of each case after tree deployment has been shown in Figure A.6 in the Appendix.

3.3.1 Overall outdoor and indoor cooling effect

The changes in outdoor and indoor thermal conditions during the simulation period with increasing TCC following the two deployment strategies are analyzed. For the overall average of building surrounding outdoor conditions and building indoor conditions, both strategies result in similar

Table 7 Number of added trees surrounding each building with T_{out_based} strategy and SET_{in_based} strategy (the building index can be referred to Fig. 6)

T_{out_based} building ranking	SET_{in_based} building ranking	Number of added trees surrounding each building					
		TCC					
		6%	9%	15%	20%	30%	40%
34	34	/	0	3	3	5	8
38	21	/	0	2	3	5	8
37	7	/	0	2	3	5	8
39	11	/	0	2	3	5	8
33	10	/	0	2	3	5	8
36	20	/	0	2	3	5	8
35	19	/	0	2	3	5	8
17	23	/	0	2	3	5	8
40	22	/	0	2	3	5	8
32	30	/	0	2	3	5	8
16	24	/	0	2	3	5	8
18	41	/	0	1	3	5	8
26	1	/	0	1	3	5	8
15	9	/	0	1	3	5	8
12	43	/	0	1	3	5	7
13	18	/	0	1	3	5	6
41	17	/	0	1	3	5	6
14	37	/	0	1	3	5	6
31	39	/	0	1	3	5	6
30	25	/	0	1	3	5	6
11	40	/	0	1	3	5	6
27	16	/	0	1	2	5	6
23	26	/	0	1	2	5	6
8	38	/	0	1	2	5	6
1	35	/	0	1	2	5	6
22	36	/	0	1	2	5	6
21	33	/	0	1	2	5	6
28	8	/	0	1	2	4	6
7	15	/	0	1	2	4	6
20	42	/	0	1	2	4	6
9	13	/	0	1	2	4	6
19	44	/	0	1	2	4	6
2	28	/	0	1	2	4	6
5	14	/	0	1	2	4	6
6	31	/	0	1	2	4	6
29	6	/	0	1	2	4	6
4	2	/	0	1	2	4	6
25	12	/	0	1	2	4	6
3	32	/	0	1	2	4	6
24	27	/	0	1	2	4	6
42	5	/	0	1	2	3	6
43	4	/	0	1	1	3	6
10	29	/	0	1	1	3	6
44	3	/	0	1	1	3	6

decreases in terms of T_{out_sur}, SET_{out_sur}, T_{in} and SET_{in}. At the TCC 30% threshold suggested by Nature Canada (Nature Canada 2022), the decreases in the average T_{out_sur}, SET_{out_sur}, T_{in} and SET_{in} are around 1.1 °C, 1.3 °C, 1.8 °C, and 1.7 °C, respectively. The difference between T and SET is due to the inclusion of additional parameters such as humidity, radiation and air speed in the SET calculation. The reductions in T_{in} and SET_{in} exceed those of T_{out_sur} and SET_{out_sur}, as tree shading significantly reduces the amount of solar radiation reaching building surfaces, thereby decreasing heat gain through windows and walls. Additionally, the buildings are designed to be well-ventilated as mentioned in Section 2.3, which enhances the cooling effect by facilitating air circulation and removing internal heat more efficiently. The relation between TCC and the average reduction of the four indices are presented in Figure A.7 in the Appendix.

Having said that, in discussions pertaining to heat stress, reductions achieved in maximum temperature or maximum heat stress are important. Figure 8 presents the maximum reductions in the four indices and their changes with TCC across the domain. As shown in Figures 8(a) and 8(b), the maximum reductions in T_{out_sur} and SET_{out_sur} are similar, with the T_{out_based} planting strategy achieving slightly higher reductions than the SET_{in_based} strategy, whereas Figures 8(c) and 8(d) illustrate that the maximum reductions in T_{in} and SET_{in} are higher in SET_{in_based} planting cases than in T_{out_based} planting cases. At TCC 30%, the maximum reduction in T_{out_sur} and SET_{out_sur} are approximately 4.0 °C and 6.9 °C, respectively, in both tree planting strategy cases. The maximum reductions in T_{in} and SET_{in} are around 5.8 °C and 5.0 °C, respectively, both occurring at 3 PM in building 07 in the SET_{in_based} case. These reductions are 5.3 °C and 4.6 °C in the T_{out_based} case, which are 0.5 °C and 0.4 °C less than in the SET_{in_based} case. Overall, in terms of average and maximum reductions, the both tree planting strategies achieve a similar extent of cooling efficiency.

3.3.2 Distribution of outdoor and indoor thermal condition

The distribution of SET_{out} at the height of 1.5 m across the neighbourhood at 2 PM for the baseline case, tree-growth case, and the eight strategic tree-planting cases are presented in Figure 9. With the increase of TCC, the SET_{out} is significantly reduced, especially under the tree canopies. Due to the varying locations of tree planting, different areas experienced SET_{out} reductions, which can be observed when TCC is less than 20%. For example, in the T_{out_based} strategy cases, significant SET_{out} reductions occur on the eastern side of the domain, while in the SET_{in_based} strategy cases, the northern side shows more pronounced reductions. This difference becomes less distinct when TCC exceeds 30%.
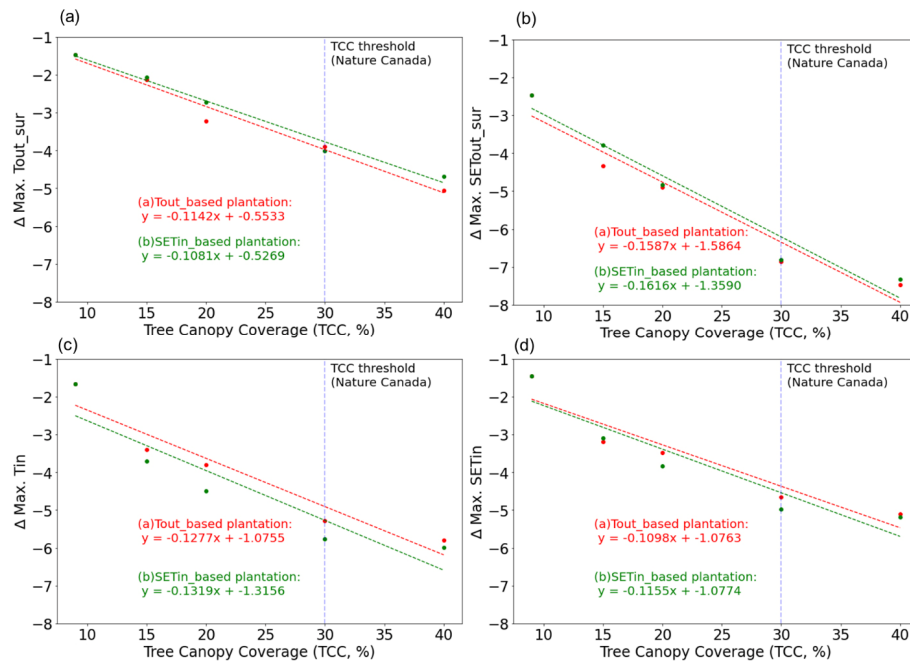
Fig. 8 Effect of increased TCC by the two tree deployment strategies on the maximum reduction of (a) T_{out_Sur}, (b) SET_{out_Sur}, (c) T_{in}, and (d) SET_{in} compared to the baseline case
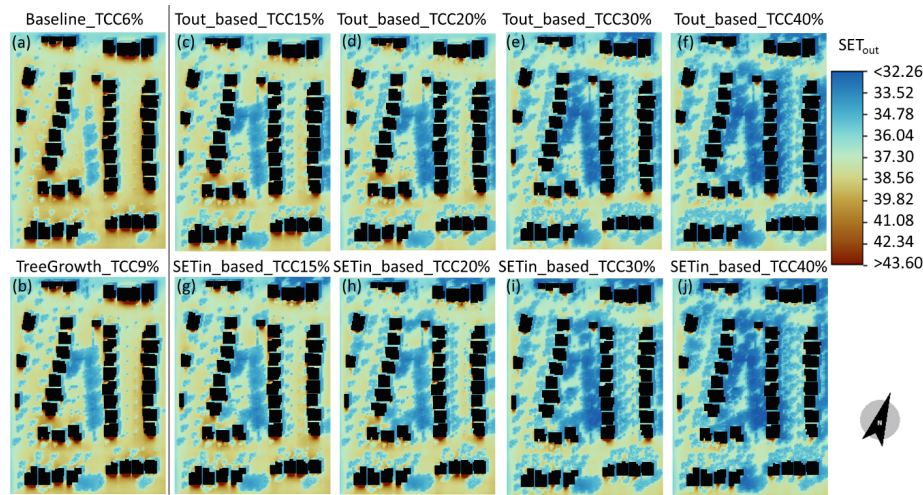

Fig. 9 Mapping of SET_{out} at 1.5 m height at 2 PM in the (a) baseline case with TCC 6%, (b) tree-growth case with TCC 9%, and T_{out_based} tree-planting cases with TCC (c) 15%, (d) 20%, (e) 30%, (f) 40%, and SET_{in_based} tree-planting cases with TCC (g) 15%, (h) 20%, (i) 30%, (j) 40%

The distribution of SET_{in} for each building at 2 PM in the baseline case, tree-growth case, and the eight strategic tree-planting cases are presented in Figure 10. In the baseline case (Figure 10(a)), buildings with higher SET_{in} located at the southeast side of the neighbourhood, which is situated on the leeward side. In this area, incoming airflow is warmed by the road and building surfaces. As shown in Figure 10(b), the indoor conditions of a limited number of buildings along the west-side road are improved due to the tree size increase. In the tree-planting cases (TCC = 15%–40%), more buildings achieve improved

indoor thermal conditions with increasing TCC. When TCC reaches 15%, the T_{out_based} strategy (Figure 10(c)) leads to greater improvement for buildings along the east-side road, compared to the SET_{in_based} strategy (Figure 10(g)), which produces more uniform improvement across the neighbourhood. At 20% TCC, the T_{out_based} strategy (Figure 10(d)) continues to enhance conditions primarily along the east-side road, while SET_{in_based} strategy consistently leads to a more uniform improvement across the neighborhood (Figure 10(h)). However, when TCC reaches 30% or higher, differences in SET_{in} distributions between
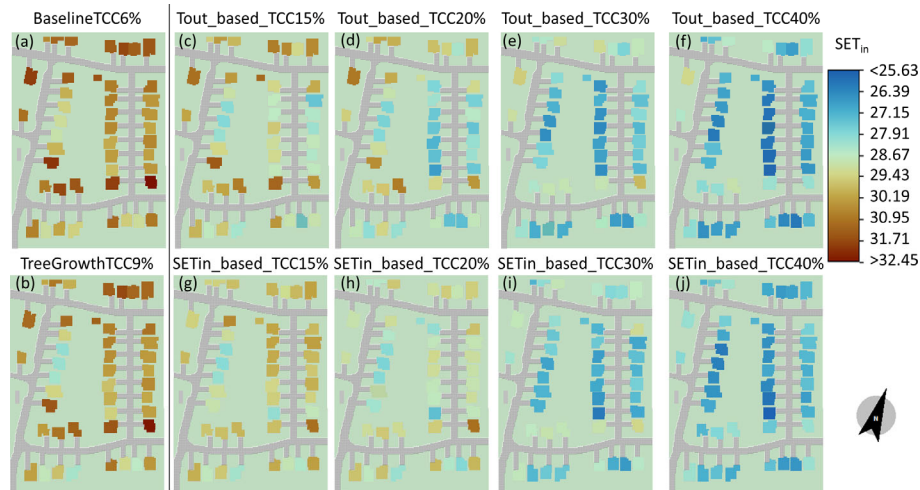
Fig. 10 Comparison of SET_{in} for each building at 2 PM in the (a) baseline case with TCC 6%, (b) tree-growth case with TCC 9%, and T_{out_based} tree-planting cases with TCC (c) 15%, (d) 20%, (e) 30%, (f) 40%, and SET_{in_based} tree-planting cases with TCC (g) 15%, (h) 20%, (i) 30%, (j) 40%

the two strategies become less pronounced. Therefore, at 2 PM, indoor thermal conditions of all buildings across the neighbourhood are improved. A difference in the spatial distribution of these improvements is observed between the two strategies under 20% TCC.

3.3.3 Distribution of building thermal resilience

In addition to the intensity of outdoor and indoor thermal stress represented by SET, it is important to incorporate the exposure time that buildings experience. To assess this, the thermal resilience performance of each building, represented by $WSETH_b$, is analyzed. Figure 11 presents the histogram of $WSETH_b$ values for all buildings in the neighbourhood across the studied cases. With increasing TCC, the histogram bars shift to left and the standard

deviation (std) become smaller, indicating that the absolute values of $WSETH_b$ decreases and become more uniform. Lower $WSETH_b$ values signify reduced building thermal stress and improved thermal resilience considering both thermal stress intensity and exposure duration. Comparing the two tree-planting strategies, although they result in similar median values of $WSETH_b$ at the same TCC, the SET_{in_based} strategy results in smaller minimum, maximum and std values, indicating a more enhanced and more uniform distribution of building thermal resilience across the neighbourhood.

To further understand the building specific thermal resilience performance, Table 8 lists the $WSETH_b$ values of each building across different cases. For the majority of buildings with higher baseline $WSETH_b$, such as buildings
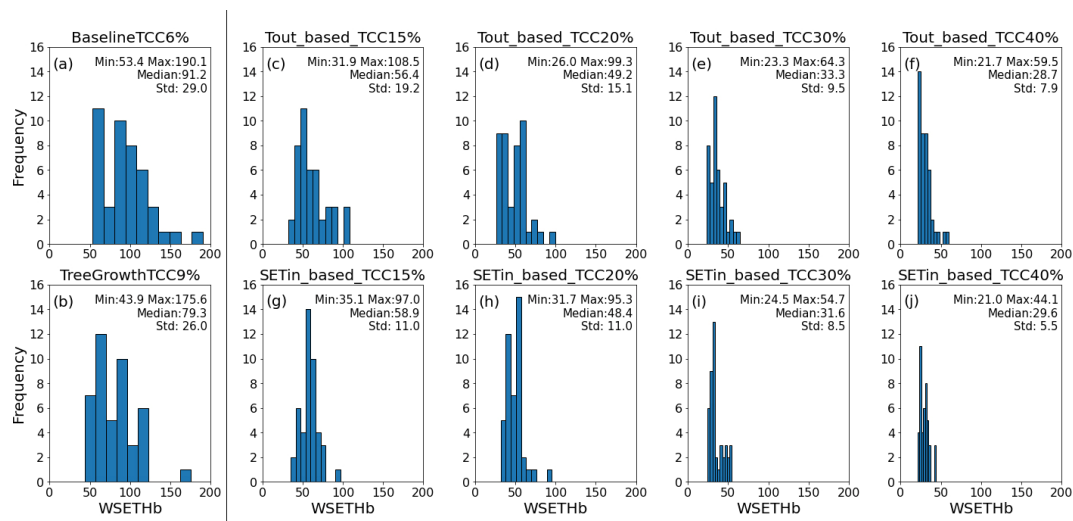

Fig. 11 Histogram and minimum (Min), maximum (Max), median, and standard deviation (std) values of building thermal resilience performance $WSETH_b$ across different cases

Table 8 Value of building thermal resilience performance *WSETH*b across different cases

Building index	WSETHb									
	TCC									
	Baseline	Tree-growth	T_{out_based} tree deployment				SET_{in_based} tree deployment			
	6%	9%	15%	20%	30%	40%	15%	20%	30%	40%
1	119.1	95.4	70.3	63.8	33.4	29.4	75.0	53.7	34.5	32.7
2	69.2	58.7	52.7	52.3	29.6	26.7	55.3	43.6	32.0	27.4
3	64.8	46.4	40.7	37.7	31.9	26.2	44.1	37.6	33.9	22.6
4	57.3	48.4	40.2	36.6	27.7	23.4	43.9	39.0	31.6	23.2
5	57.8	48.8	42.4	34.7	24.9	22.8	42.1	35.0	30.5	23.7
6	75.9	60.5	58.4	52.0	34.4	31.7	53.0	45.6	31.6	24.1
7	152.6	113.8	106.2	75.0	35.8	31.8	54.9	43.2	30.3	30.0
8	92.7	72.3	63.0	56.0	40.9	35.6	61.0	54.7	43.4	31.3
9	123.6	93.1	64.3	55.4	44.5	35.0	63.2	55.3	48.1	31.5
10	100.5	98.7	78.3	77.5	44.1	41.5	57.9	47.4	40.4	32.4
11	120.9	96.8	90.5	55.0	44.1	35.3	57.7	55.5	46.8	32.6
12	60.4	53.1	41.0	26.0	23.3	21.7	35.1	31.7	24.5	21.0
13	64.0	58.5	53.0	33.4	26.9	23.2	56.3	42.4	25.4	24.6
14	63.7	59.2	48.8	30.4	26.1	24.6	53.3	41.1	26.8	23.0
15	81.8	63.6	55.3	34.0	23.7	23.5	59.5	48.8	27.7	25.4
16	91.2	63.4	43.0	31.4	25.0	23.5	62.5	53.5	26.3	23.9
17	97.8	90.1	48.4	42.8	31.8	23.2	71.4	46.9	31.4	24.1
18	91.2	91.1	57.4	37.7	28.2	28.2	68.0	39.8	29.6	25.0
19	129.1	114.4	108.5	57.1	31.6	25.7	58.7	36.5	30.2	27.4
20	109.5	106.0	91.1	62.2	53.6	45.1	63.0	54.5	44.1	30.2
21	115.0	111.7	78.5	55.6	39.1	29.4	46.5	55.2	31.5	24.8
22	100.2	96.1	54.8	38.2	32.4	25.4	58.9	40.5	31.1	25.0
23	106.2	92.6	68.8	58.1	39.8	33.7	59.7	51.9	38.5	29.7
24	140.6	110.2	107.3	99.3	64.3	59.5	63.7	53.4	52.0	43.4
25	106.4	88.5	78.9	57.2	55.1	52.1	65.5	53.7	47.4	42.2
26	109.6	83.8	70.0	51.7	43.5	39.3	73.0	60.3	51.0	44.1
27	53.4	47.9	45.5	36.0	29.8	24.2	45.5	44.0	30.9	28.9
28	73.7	62.3	58.1	53.7	32.6	26.0	58.3	56.1	30.9	30.4
29	58.4	43.9	42.2	38.7	28.9	24.9	41.0	39.1	32.4	25.8
30	129.0	110.5	85.7	50.2	46.2	33.9	78.0	71.4	50.6	32.2
31	56.4	60.4	51.0	32.2	26.0	22.8	52.2	43.9	30.0	25.5
32	55.0	49.4	34.9	33.0	25.1	24.8	45.7	35.4	25.2	24.1
33	89.1	64.4	48.1	46.4	38.7	29.5	67.9	58.9	40.8	37.1
34	190.1	175.6	69.8	71.1	57.3	36.2	97.0	95.3	54.7	36.5
35	86.1	79.4	50.5	33.1	32.3	24.5	53.5	48.0	29.4	29.9
36	82.3	78.5	48.1	42.9	33.1	26.1	61.4	55.3	31.6	27.5
37	97.7	88.9	51.3	40.0	33.6	29.4	59.4	48.7	32.6	33.1
38	82.2	79.1	44.1	32.6	32.5	26.1	63.5	52.1	30.3	30.7
39	83.2	83.8	49.3	48.2	36.3	30.1	63.7	55.0	31.8	32.6
40	66.3	65.3	31.9	32.8	32.4	27.1	64.3	44.2	27.4	29.5
41	112.8	110.8	73.2	57.4	38.0	32.5	69.8	63.7	52.7	33.4
42	90.2	60.6	58.2	53.7	43.8	29.2	57.7	48.2	29.7	29.5
43	95.5	82.6	64.2	61.1	37.3	30.7	57.9	39.7	32.3	32.4
44	94.5	60.7	58.3	59.9	48.3	37.8	59.0	54.6	41.8	35.7

#7, #9, #11, #19, #24, and #30, the SET_{in_based} strategy achieves greater reduction, especially at TCC 15% and 20%. For buildings with moderate or low baseline $WSETH_b$, such as buildings #1 and #2, two strategies achieve comparable reductions, with the T_{out_based} strategy slightly outperforming the SET_{in_based} strategy, especially at TCC 30% and 40%. For the building #34, which has the highest baseline $WSETH_b$, even the same number of trees are deployed by the two strategies at each TCC level (referring to Table 7), the achieved reduction in $WSETH_b$ differs. This indicates that the enhancement of a building's thermal resilience is not solely determined by the trees deployed around that building but is also influenced by the tree deployment around neighboring buildings and the overall neighborhood deployment. At 30% TCC and above, both strategies achieved similar $WSETH_b$ for building #34, suggesting that at TCC levels higher than 30%, the specific tree deployment prioritization strategy becomes less critical, which aligns with the findings discussed in Section 3.3.2.

4 Discussions and conclusions

4.1 Discussions

The method used in this study ensures that the building thermal performance indicator is influenced by urban morphology, urban greenery, microclimate, and building performance. The indicator is used to calculate the thermal resilience index, considering the building thermal performance failure intensity and recovery time from heatwaves based on the concept of resilience. This method can be extensively used to evaluate other cooling strategies at both the building and neighbourhood levels, providing a better understanding of the strategies' efficiency in improve thermal resilience. It can also be applied to other scenarios, such as power outage in both cooling and heating seasons, to assess neighbourhood resilience to grid failure and enhance its reliability.

This study uses an archetype building model to represent the general situation of buildings due to a lack of detailed information for all houses in the studied neighbourhood. This model is designed to be well-ventilated, when combined with the shading effects of trees, results in a greater reduction in T_{in} compared to T_{out} when increasing TCC. Future studies could conduct surveys of each building and consider individual building features' impact on indoor thermal conditions. In microclimate and building co-simulations, the convective heat transfer coefficient (CHTC) within the building model can be adjusted based on microclimate simulation results, particularly when wind speed and direction significantly impact building infiltration and natural

ventilation. This can be achieved using the built-in airflow network module in EnergyPlus.

Although air temperature and SET are used in this study to represent outdoor and indoor thermal conditions, other occupant vulnerability metrics, such as operative temperature, humidity, heat index and so on, can also be used depending on the importance and availability of the environmental and physiological parameters. Policymakers, urban planners and public health agencies can benefit from the thermal resilience quantification method as it enables informed decision-making when proposing new codes, standards, and social protection programs. Additionally, system vulnerability metrics, financial metrics, and energy performance metrics could also be integrated into the proposed framework, benefitting a broader range of stakeholders, including mechanical and civil engineers, real estate developers, corporate building owners and insurance companies (Hong et al. 2023).

The findings of this study demonstrate that the T_{out_based} and SET_{in_based} strategic tree deployment can significantly enhance neighbourhood thermal resilience. Although similar average and maximum cooling effects in the neighbourhood are observed by both strategies, the SET_{in_based} shows superior performance under TCC 20%, by promoting a more uniform distribution of thermal conditions and resilience across the neighborhood and providing greater thermal resilience for some buildings with poorer baseline conditions. As TCC exceeds 30%, the spatial distribution differences between the two strategies diminish, resulting in comparable outcomes and a more consistent resilience level across all buildings. At these higher TCC levels, deploying trees in outdoor hotspots is a practical and acceptable strategy, eliminating the need for detailed indoor condition measurements or simulations.

To further understand the mechanism of microclimate/ indoor interactions, sensitivity analysis can evaluate the relative impacts of tree-induced shading, radiation trapping, cooling and humidifying effects on building thermal resilience. Various statistical and machine learning approaches can be utilized to explore the relationships and the significance of each outdoor parameter, ensuring a comprehensive understanding of these interactions.

4.2 Conclusions

This study evaluated the effectiveness of tree deployment strategies, and identified best practices to improve the thermal resilience of buildings across a neighborhood in the city of London in Canada. The consistency of prioritized buildings for tree deployment, based on outdoor and indoor conditions, is assessed using Kendall's Tau and the

associated *p*-values. The two strategies to deploy urban trees include adding trees based on outdoor high-temperature hotspots ($T_{\text{out\_based}}$) and high indoor heat stress ($\text{SET}_{\text{in\_based}}$), respectively. Tree growth and its influence on canopy coverage is also considered. The effects of trees on the outdoor environment are simulated with the ENVI-met model, whereas the modelling of indoor environment is performed using the EnergyPlus. The ENVI-met model was evaluated with traverse measurement data and the performance is comparable to previous evaluations of the model. The outdoor and indoor thermal conditions are evaluated with air temperature and SET. The building thermal resilience is evaluated accounting for the influence of microclimate, and considering both heat stress intensity and exposure time. Following conclusions can be made from the results obtained in this study:

- The building rankings based on outdoor hotspots and indoor heat stress are inconsistent, leading to different prioritized locations for tree deployment under the $T_{\text{out\_based}}$ strategy and $\text{SET}_{\text{in\_based}}$ strategies.

- When TCC is increased from the baseline level (6%) to 30%—a level recommended by Nature Canada—the maximum reductions in building surrounding temperature and SET are approximately 4.0 °C and 6.9 °C, respectively, with both tree deployment strategies. The maximum reductions in indoor temperature and SET are around 5.8 °C and 5.0 °C with $\text{SET}_{\text{in\_based}}$ strategy, and around 5.3 °C and 4.6 °C with $T_{\text{out\_based}}$ strategy. Both tree deployment strategies achieve a comparable extent of cooling efficiency in terms of average and maximum temperature and SET reductions across the neighbourhood.

- In the studied neighbourhood, cooling effects from grown trees can be greater than young trees by up to 1.5 °C and 1.7 °C for outdoor and indoor temperatures, respectively.

- At TCC levels of 20% and below, the $\text{SET}_{\text{in\_based}}$ strategy achieves a more uniform distribution of thermal conditions and resilience across the neighborhood, and greater thermal resilience for the majority of buildings with poorer baseline conditions. As TCC levels exceed 30%, the differences between the two strategies become less pronounced, resulting in comparable thermal outcomes and a uniform resilience level across all buildings.

- When space in a neighbourhood for tree deployment is limited, the $\text{SET}_{\text{in\_based}}$ strategy is recommended for achieving enhanced and uniformly distributed thermal resilience. However, when TCC 30% is achievable, deploying trees based on outdoor temperature hotspots is a straightforward yet effective strategy for improving neighborhood thermal resilience.

- The enhancement in thermal resilience of an individual building is influenced not only by the trees deployed around it but also by the tree configuration and deployment in neighboring buildings and the overall neighborhood.

In the future, the current strategy of increasing TCC combining with other resilient cooling strategies such as green roofs/walls, cool roofs, will be investigated to achieve higher thermal resilience in this community. Furthermore, the method proposed in this work can be expanded to other types of communities and various heatwave scenarios, and the efficiency of these cooling strategies can be investigated under future projected heat events in the communities.

Data deposition information

Acknowledgements

Declaration of competing interest

The authors have no competing interests to declare that are relevant to the content of this article.

Author contribution statement

All authors contributed to the study conception and design. Material preparation, data collection and analysis were performed by Lili Ji, Abhishek Gaur, James Voogt and E. Scott Krayenhoff. The first draft of the manuscript was written by Lili Ji and all authors commented on previous versions of the manuscript. All authors read and approved the final manuscript.

References

Amitrano C, Arena C, Rouphael Y, et al. (2019). Vapour pressure deficit: The hidden driver behind plant morphofunctional traits in controlled environments. *Annals of Applied Biology*, 175: 313–325.

ASHRAE (2017). ANSI/ASHRAE Standard - 55. Thermal environmental conditions for human occupancy. Atlanta, GA, USA: American Society of Heating, Refrigerating and Air-Conditioning Engineers.

Astell-Burt T, Feng X (2020a). Does sleep grow on trees? A longitudinal study to investigate potential prevention of insufficient sleep with different types of urban green space. *SSM - Population Health*, 10: 100497.

Astell-Burt T, Feng X (2020b). Urban green space, tree canopy and prevention of cardiometabolic diseases: A multilevel longitudinal study of 46 786 Australians. *International Journal of Epidemiology*, 49: 926–933.

Attia S, Levinson R, Ndongo E, et al. (2021). Resilient cooling of buildings to protect against heat waves and power outages: Key concepts and definition. *Energy and Buildings*, 239: 110869.

Birkmann J, Jamshed A, McMillan JM, et al. (2022). Understanding human vulnerability to climate change: A global perspective on index validation for adaptation planning. *Science of the Total Environment*, 803: 150065.

Cabinet Office (2011). Keeping the country running: Natural hazards and infrastructure. Improving the UK's ability to absorb, respond to and recover from emergencies.

Coutts AM, White EC, Tapper NJ, et al. (2016). Temperature and human thermal comfort effects of street trees across three contrasting street canyon environments. *Theoretical and Applied Climatology*, 124: 55–68.

Darvish A, Eghbali G, Eghbali SR (2021). Tree-configuration and species effects on the indoor and outdoor thermal condition and energy performance of courtyard buildings. *Urban Climate*, 37: 100861.

DOE (2024). EnergyPlus. US Department of Energy.

Elraouf RA, ELMokadem A, Megahed N, et al. (2022). Evaluating urban outdoor thermal comfort: a validation of ENVI-met simulation through field measurement. *Journal of Building Performance Simulation*, 15: 268–286.

ENVI-met (2024). ENVI-met. Available at https://www.envi-met.com

Environment Canada (2024). Historical Data. Available at https://climate.weather.gc.ca/historical_data/search_historic_data_e.html. Accessed 5 Jun 2024.

Erell E, Zhou B (2022). The effect of increasing surface cover vegetation on urban microclimate and energy demand for building heating and cooling. *Building and Environment*, 213: 108867.

Ge J, Wang Y, Akbari H, et al. (2023). Cooling energy saving by vegetation planting in high-density districts: Evaluation using the coupled simulation. *Building and Environment*, 232: 110054.

Guo W, Liang S, He Y, et al. (2022). Combining EnergyPlus and CFD to predict and optimize the passive ventilation mode of medium-sized gymnasium in subtropical regions. *Building and Environment*, 207: 108420.

Hadavi M, Pasdarshahri H (2021). Impacts of urban buildings on microclimate and cooling systems efficiency: Coupled CFD and BES simulations. *Sustainable Cities and Society*, 67: 102740.

Hao T, Zhao Q, Huang J (2023). Optimization of tree locations to reduce human heat stress in an urban park. *Urban Forestry & Urban Greening*, 86: 128017.

Homaei S, Hamdy M (2021). Thermal resilient buildings: How to be quantified? A novel benchmarking framework and labelling metric. *Building and Environment*, 201: 108022.

Hong T, Malik J, Krelling A, et al. (2023). Ten questions concerning thermal resilience of buildings and occupants for climate adaptation. *Building and Environment*, 244: 110806.

Hsieh CM, Li J, Zhang L, et al. (2018). Effects of tree shading and transpiration on building cooling energy use. *Energy and Buildings*, 159: 382–397.

Huang H, Xie W, Sun H (2015). Simulating 3D urban surface temperature distribution using ENVI-MET model: Case study on a forest park. In: Proceedings of 2015 IEEE International Geoscience and Remote Sensing Symposium (IGARSS, Milan, Italy).

Iungman T, Cirach M, Marando F, et al. (2023). Cooling cities through urban green infrastructure: a health impact assessment of European cities. *The Lancet*, 401: 577–589.

Jaffal I, Ouldboukhitine SE, Belarbi R (2012). A comprehensive study of the impact of green roofs on building energy performance. *Renewable Energy*, 43: 157–164.

Ji L, Shu C, Laouadi A, et al. (2023). Quantifying improvement of building and zone level thermal resilience by cooling retrofits against summertime heat events. *Building and Environment*, 229: 109914.

Ji L, Shu C, Gaur A, et al. (2024). A state-of-the-art review of studies on urban green infrastructure for thermal resilient communities. *Building and Environment*, 257: 111524.

Konijnendijk CC (2023). Evidence-based guidelines for greener, healthier, more resilient neighbourhoods: Introducing the 3-30-300 rule. *Journal of Forestry Research*, 34: 821–830.

Kottek M, Grieser J, Beck C, et al. (2006). World map of the Köppen-Geiger climate classification updated. *Meteorologische Zeitschrift*, 15: 259–263.

Krayenhoff ES, Moustaoui M, Broadbent AM, et al. (2018). Diurnal interaction between urban expansion, climate change and adaptation in US cities. *Nature Climate Change*, 8: 1097–1103.

Krayenhoff ES, Jiang T, Christen A, et al. (2020). A multi-layer urban canopy meteorological model with trees (BEP-Tree): Street tree impacts on pedestrian-level climate. *Urban Climate*, 32: 100590.

Krayenhoff ES, Broadbent AM, Zhao L, et al. (2021). Cooling hot cities: a systematic and critical review of the numerical modelling literature. *Environmental Research Letters*, 16: 053007.

Krelling AF, Lamberts R, Malik J, et al. (2023). A simulation framework for assessing thermally resilient buildings and communities. *Building and Environment*, 245: 110887.

Laouadi A, Gaur A, Lacasse MA, et al. (2020). Development of reference summer weather years for analysis of overheating risk in buildings. *Journal of Building Performance Simulation*, 13: 301–319.

Laouadi A, Bartko M, Gaur A, et al. (2022). Guideline for management of overheating risk in residential buildings.

Li Y, Lin D, Zhang Y, et al. (2023). Quantifying tree canopy coverage threshold of typical residential quarters considering human thermal comfort and heat dynamics under extreme heat. *Building and Environment*, 233: 110100.

Lindenmayer A (1968). Mathematical models for cellular interactions in development II. Simple and branching filaments with two-sided inputs. *Journal of Theoretical Biology*, 18: 300–315.

Locke DH, Baker M, Alonzo M, et al. (2024). Variation the in relationship between urban tree canopy and air temperature reduction under a range of daily weather conditions. *Heliyon*, 10: e25041.

Lu H, Gaur A, Krayenhoff ES, et al. (2023). Thermal effects of cool roofs and urban vegetation during extreme heat events in three Canadian regions. *Sustainable Cities and Society*, 99: 104925.

Makvandi M, Li B, Elsadek M, et al. (2019). The interactive impact of building diversity on the thermal balance and micro-climate change under the influence of rapid urbanization. *Sustainability*, 11: 1662.

McPherson EG, Herrington LP, Heisler GM (1988). Impacts of vegetation on residential heating and cooling. *Energy and Buildings*, 12: 41–51.

Meili N, Manoli G, Burlando P, et al. (2021). Tree effects on urban microclimate: Diurnal, seasonal, and climatic temperature differences explained by separating radiation, evapotranspiration, and roughness effects. *Urban Forestry & Urban Greening*, 58: 126970.

Morakinyo TE, Lam YF (2016). Simulation study on the impact of tree-configuration, planting pattern and wind condition on street-canyon's micro-climate and thermal comfort. *Building and Environment*, 103: 262–275.

Muñoz-Pichardo JM, Lozano-Aguilera ED, Pascual-Acosta A, et al. (2021). Multiple ordinal correlation based on Kendall's tau measure: A proposal. *Mathematics*, 9: 1616.

Natural Resources Canada (2022). Canadian Weather Energy and Engineering Datasets (CWEEDS). Available at https://open.canada.ca/data/en/dataset/005494f2-1848-48d5-abe4-a76a7846f035. Accessed 5 Jun 2024.

Nature Canada (2022). Nature-Canada-Report-Tree-Equity.

NRC (2015). National Building Code of Canada 2015. Ottawa.

NRC (2017). National Energy Code of Canada for Buildings. Canadian Commission on Building and Fire Codes. Available at https://nrc.canada.ca/en/certifications-evaluations-standards/codes-canada/codes-canada-publications/national-energy-code-canada-buildings-2017.

Ouyang W, Morakinyo TE, Ren C, et al. (2020). The cooling efficiency of variable greenery coverage ratios in different urban densities: A study in a subtropical climate. *Building and Environment*, 174: 106772.

Rahif R, Hamdy M, Homaei S, et al. (2022). Simulation-based framework to evaluate resistivity of cooling strategies in buildings against overheating impact of climate change. *Building and Environment*, 208: 108599.

Shaamala A, Yigitcanlar T, Nili A, et al. (2024). Algorithmic green infrastructure optimisation: Review of artificial intelligence driven approaches for tackling climate change. *Sustainable Cities and Society*, 101: 105182.

Shu C, Wang C, Xu J, et al. (2016). Microclimate modelling of typical land use units with different arrangements: A case study in Langfang. In: Proceedings of the 8th Asian Conference on Refrigeration and Air Conditioning (ACRA2016).

Shu C, Gaur A, Wang LL, et al. (2022). Added value of convection permitting climate modelling in urban overheating assessments. *Building and Environment*, 207: 108415.

Shu C, Gaur A, Lacasse M, et al. (2023a). Interaction between the urban heat island effect and the occurrence of heatwaves: Comparison of days with and without heatwaves. In: Proceedings of the 5th International Conference on Building Energy and Environment.

Shu C, Gaur A, Wang L, et al. (2023b). Evolution of the local climate in Montreal and Ottawa before, during and after a heatwave and the effects on urban heat islands. *Science of the Total Environment*, 890: 164497.

Shu C, Xie Z, Ji L, et al. (2023c). Comparing multiple overheating assessment metrics using measured data. In: Proceedings of the 5th International Conference on Building Energy and Environment.

Simon H (2016). Modeling urban microclimate: Development, implementation and evaluation of new and improved calculation methods for the urban microclimate model ENVI-met.

Sinsel T (2021). Advancements and applications of the microclimate model ENVI-met. der Johannes Gutenberg-Universität Mainz.

Stastny A, Voogt JA, Lao J (2023). A mobile traverse method to measure neighbourhood-scale microclimate. *Proceedings of the 5th International Conference on Building Energy and Environment*. Springer Nature Singapore, pp 2821–2824.

Tsoka S, Leduc T, Rodler A (2021). Assessing the effects of urban street trees on building cooling energy needs: The role of foliage

density and planting pattern. *Sustainable Cities and Society*, 65: 102633.

Wang H, Peng C, Li W, et al. (2021). Porous media: A faster numerical simulation method applicable to real urban communities. *Urban Climate*, 38: 100865.

Wu Z, Dou P, Chen L (2019). Comparative and combinative cooling effects of different spatial arrangements of buildings and trees on microclimate. *Sustainable Cities and Society*, 51: 101711.

Yang X, Zhao L, Bruse M, et al. (2013). Evaluation of a microclimate model for predicting the thermal behavior of different ground surfaces. *Building and Environment*, 60: 93–104.

Yang Y, Zhang X, Lu X, et al. (2018). Effects of building design elements on residential thermal environment. *Sustainability*, 10: 57.

Yang J, Hu X, Feng H, et al. (2021). Verifying an ENVI-met simulation of the thermal environment of Yanzhong Square Park in Shanghai. *Urban Forestry & Urban Greening*, 66: 127384.

Zhang C, Kazanci OB, Levinson R, et al. (2021). Resilient cooling strategies—A critical review and qualitative assessment. *Energy and Buildings*, 251: 111312.

Zheng X, Chen L, Yang J (2023). Simulation framework for early design guidance of urban streets to improve outdoor thermal comfort and building energy efficiency in summer. *Building and Environment*, 228: 109815.

Zhu S, Li Y, Wei S, et al. (2022). The impact of urban vegetation morphology on urban building energy consumption during summer and winter seasons in Nanjing, China. *Landscape and Urban Planning*, 228: 104576.

Ziter CD, Pedersen EJ, Kucharik CJ, et al. (2019). Scale-dependent interactions between tree canopy cover and impervious surfaces reduce daytime urban heat during summer. *Proceedings of the National Academy of Sciences of the United States of America*, 116: 7575–7580.